ChemSusChem

Research Article
doi.org/10.1002/cssc.202301534

Chemistry Europe
European Chemical Societies Publishing

www.chemsuschem.org

Perovskite for Electrocatalytic Oxygen Evolution at Elevated Temperatures

Fatma Abdelghafar,[a, b] Xiaomin Xu,*[a] San Ping Jiang,[a, c] and Zongping Shao*[a]

The development of advanced electrolysis technologies such as anion exchange membrane water electrolyzer (AEMWE) is central to the vision of a sustainable energy future. Key to the realization of such AEMWE technology lies in the exploration of low-cost and high-efficient catalysts for facilitating the anodic oxygen evolution reaction (OER). Despite tremendous efforts in the fundamental research, most of today's OER works are conducted under room temperature, which deviates significantly with AEMWE's operating temperature (50–80 °C). To bridge this gap, it is highly desirable to obtain insights into the OER catalytic behavior at elevated temperatures. Herein, using the well-known perovskite catalyst $Ba_{0.5}Sr_{0.5}Co_{0.8}Fe_{0.2}O_{3-\delta}$ (BSCF) as a proof of concept, the effect of temperature on the variation in OER catalytic activity and stability is evaluated. It is found that the BSCF's activity increases with increasing temperature due to enhanced lattice oxygen participation promoting the lattice oxygen-mediated OER process. Further, surface amorphization and cation leaching of BSCF become more pronounced as temperature increases, causing a somewhat attenuated OER stability. These new understandings of the fundamental OER catalysis over perovskite materials at industrial-relevant temperature conditions are expected to have strong implications for the research of OER catalysts to be deployed in practical water electrolyzers.

Introduction

The advancement of renewable energy sources is crucial for contemporary human civilization and sustainable development because the use of the traditional fossil fuels today not only damages the environment but also exacerbates climate change.[1] Although solar and wind power are viable energy sources, their intermittent nature means that there can be a gap between demand and consumption even when using renewable sources. Interestingly, electrochemical energy conversion technologies such as electrolysis can fill this gap.[2] Notably, water electrolysis, when powered by renewables-generated electricity, can turn cheap, abundant water molecules into green hydrogen as a useful fuel or energy carrier.[3] There are generally three types of electrolyzers for the electrolysis of liquid water, namely the alkaline water electrolyzer (AWE),[4] proton exchange membrane water electrolyzer (PEMWE),[5] and anion exchange membrane water electrolyzer (AEMWE).[6] AEMWE is particularly promising because it combines the advantages of the former two, having a zero-gap membrane separator like a PEMWE does and allowing the use of non-precious metal catalysts as in an AWE.[7] Despite some recent advances, there is still much room for efficiency improvements of AEWME, especially in regard to the creation of cost-effective and high-efficient catalysts to replace the noble metal-based counterparts for both the cathodic hydrogen evolution reaction and, more notably, the anodic oxygen evolution reaction (OER).[8]

The OER is an intricate four-electron oxidation process ($4OH^- \rightarrow O_2 + 2H_2O + 4e^-$) with a tremendously challenging energy barrier, substantially restricting the overall water splitting efficiency.[9] Over the years, important breakthroughs have been made in the fundamental research of various types of candidate materials for catalyzing the OER, among which perovskite oxides based on non-noble metals have arisen as a significant category of functional materials for efficient OER catalysis.[10] One best-known characteristic of perovskite oxides lies in their chemical, compositional, and structural flexibility enabling a high degree of tunability in the physicochemical properties, which is highly suited for the rational design of OER catalysts. A typical example is the discovery of an activity descriptor based on the molecular orbital principles, called e_g occupancy of the surface transition metal cations of perovskite oxides, which identifies $Ba_{0.5}Sr_{0.5}Co_{0.8}Fe_{0.2}O_{3-\delta}$ (BSCF) with $e_g \approx 1$ to be a high-performing candidate showing better intrinsic activity than the iridium oxide standard.[11] This has later inspired extensive and intensive research on the exploration of perovskite oxides including both BSCF and beyond.[10,12] While substantial progress has been achieved, it should be noted that

[a] F. Abdelghafar, Dr. X. Xu, Prof. Dr. S. P. Jiang, Prof. Dr. Z. Shao
WA School of Mines: Minerals, Energy and Chemical Engineering (WASM-MECE)
Curtin University
Perth, WA, 6102, Australia
E-mail: xiaomin.xu@curtin.edu.au
zongping.shao@curtin.edu.au

[b] F. Abdelghafar
Department of Evaluation and Analysis
Egyptian Petroleum Research Institute
Cairo, 11727, Egypt

[c] Prof. Dr. S. P. Jiang
Foshan Xianhu Laboratory of the Advanced Energy Science and Technology
Guangdong Laboratory
Foshan, 528216, China

Supporting information for this article is available on the WWW under https://doi.org/10.1002/cssc.202301534

the vast majority of the OER works, including those on perovskite oxide catalysts, focus on catalytic behavior at ambient temperature. The impact of temperature on OER performance remains largely underexplored, presenting a huge gap between fundamental research and practical applications such as in AEMWE which usually operates at elevated temperatures of 50–80 °C.[13] Again, taking BSCF as an example, research following its discovery has solely centered on its OER catalysis at room temperature,[14] despite one report on the use of a BSCF nanoparticulate catalyst in an AEMWE operated at 50 °C.[15] Considering the development of BSCF as an example of non-precious metal OER catalysts, researching their intrinsic catalytic activity and stability at elevated temperatures close to the industrial operating environment represents a crucial step toward overcoming the limitations in the development of efficient AEMWE devices.

In this work, we evaluate the impact of elevating the operating temperature as an alternative perspective to developing new catalysts for improved OER catalysis. For this purpose, the BSCF perovskite oxide was selected as a candidate catalyst and appraised for the OER activity and stability at various temperatures (25, 40, 50, and 60 °C). Our results demonstrate that the BSCF's activity increases with increasing temperature, which is likely due to the enhanced lattice oxygen participation at elevated temperatures. Further, BSCF is found to become less catalytically stable with increasing temperature, which is associated with the surface amorphization and cation leaching of BSCF that become more severe as temperature is elevated. These findings offer new insights into the fundamental OER catalysis of perovskite materials at temperature conditions relevant to practical water electrolyzers such as systems like the AEMWE. This study may serve as an example of investigating the activity and stability of OER catalysts under near-industrial conditions.

Results and Discussion

The BSCF sample was prepared by a conventional sol–gel method. The X-ray diffraction (XRD) data, as presented in Figure S1, confirmed the simple cubic phase structure of BSCF (symmetry: $Pm\bar{3}m$).[14c] The electrocatalytic OER activity of the as-prepared BSCF was then investigated under varying temperatures using a rotating disk electrode (RDE) setup equipped with a water-jacketed electrolytic cell whose temperature was controlled by a thermostatic water bath circulator.[16] The BSCF catalyst was immobilized on a glassy carbon electrode (GCE) featuring a polyether ether ketone (PEEK) shroud to allow operation within the temperature range of 25–60 °C. Figure 1a shows the OER kinetic current versus overpotential as a function of temperature for the BSCF in a 1 M KOH electrolyte. Here, overpotential (η) is described as the disparity between the applied potential and the equilibrium potential (dependent on temperature, see Experimental Section); the smaller the overpotential, the better the OER activity. Noticeably, the current density at a given overpotential was found to increase with temperature. More specifically, as displayed in Figure 1b, raising

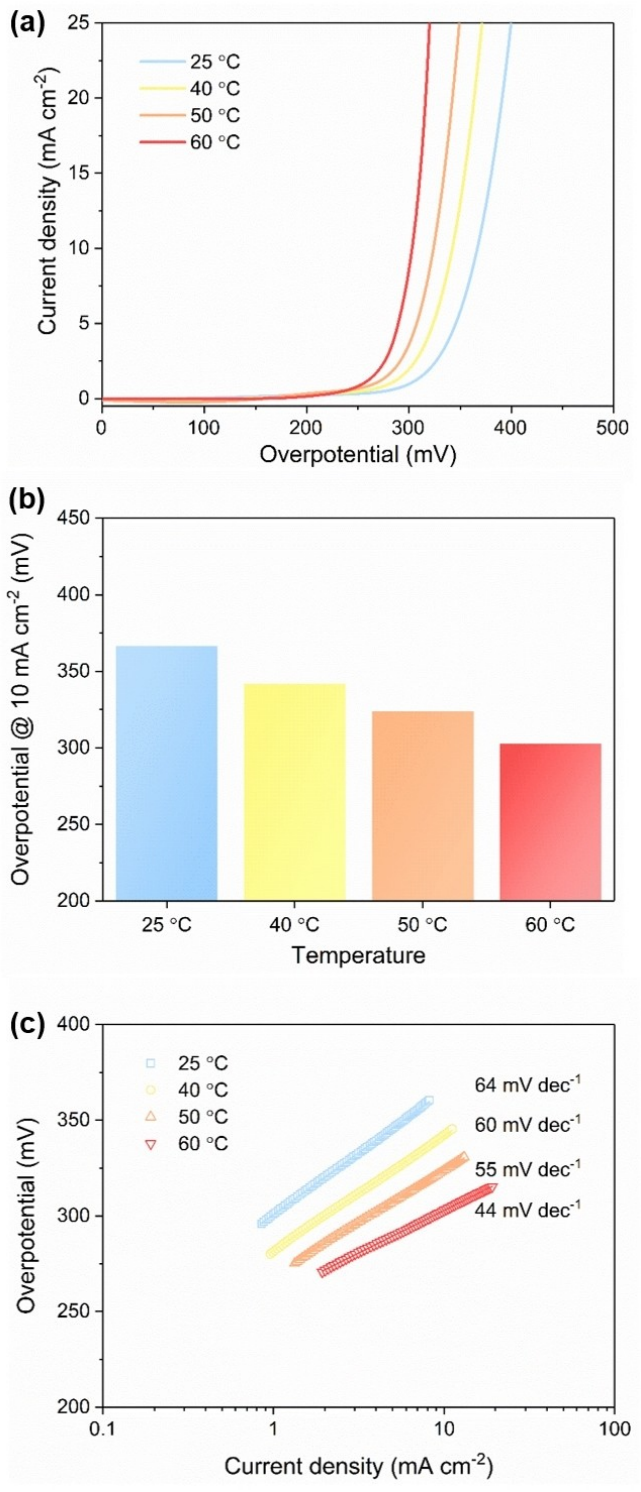

Figure 1. Enhanced OER activity of BSCF in 1 M KOH at elevated temperatures. (a) OER kinetic currents. (b) Comparison of overpotential at a current density of 10 mA cm^{-2}. (c) Tafel plots.

the electrolyte temperature from 25 to 60 °C leads to a considerable reduction of the overpotential required to achieve a current density of 10 mA cm^{-2} (from 367 to 303 mV), corresponding to a notable enhancement in the OER activity. These observations suggest that the OER over the BSCF

perovskite is highly sensitive to the changes in temperature. Figure 1c compiles Tafel analyses of the OER in 1 M KOH where linear relations between the logarithm of current density and overpotential were observed for all temperature regimes. As temperature increases, the Tafel slope was found to decrease to some extent (from 64 mV dec^{-1} at 25 °C to 44 mV dec^{-1} at 60 °C). The decrease of Tafel slope represents another indication of the improved OER kinetics for BSCF at elevated temperatures and, according to the literature,[17] could be attributed to a change in the OER mechanism or pathway (which will be further discussed below). Noteworthy, similar findings were observed when the OER over BSCF was evaluated in different alkaline electrolytes (i.e., 0.1 M and 6 M KOH, Figures S2 and S3). All these results confirm that raising the operating temperature can be an efficient strategy for improving the electrocatalytic OER activity of the BSCF catalyst.

It is important to understand the fundamental origin of the substantially improved OER kinetics of BSCF at elevated temperatures. Previous research has suggested that the OER over the BSCF oxide could follow a lattice oxygen-mediated mechanism (LOM) where oxygen anions coming from the BSCF lattice directly participate in the reaction.[14g,15] Considering that the OER for an oxide catalyst exhibiting the LOM character would show a pH dependence when the overpotential is constant,[18] we studied the pH effect on the OER activity of BSCF at different temperatures. As depicted in Figure 2a, the OER currents at constant overpotentials increased with increasing pH at each operating temperature. It suggests that the pH dependence of the OER kinetics holds for all the temperature conditions investigated, hence supporting the operation of the LOM pathway. Of note, such pH dependence became more pronounced with increasing temperature. This is especially the case when one compares the OER activity at a select overpotential of 300 mV (Figure 2b). Furthermore, the proton reaction order (*n*) could be derived from the slope of the linear relationships between the logarithm of current density (*j*) and pH when overpotential is held constant,[18b] as given below:

$$n = \left(\frac{\partial \log(j)}{\partial \mathrm{pH}}\right)_{\eta} \quad (1)$$

Of note, the proton reaction order can serve as a metric to assess the tendency of the LOM involvement; the larger the proton reaction order, the greater the LOM involvement.[18a,19] From Figure 2b, *n* values in the range of 0.40–0.70 could be obtained, which compare well to those for other Co-based perovskite oxides reported to catalyze the OER via the LOM mechanism.[19,20] Specifically, *n* at temperatures of 25, 40, 50, and 60 °C was calculated to be 0.43, 0.46, 0.55, and 0.62, respectively. The increase in proton reaction order as temperature rises implies a greater preference for the LOM at higher temperatures, thus leading to enhanced OER activity.

To further corroborate the lattice oxygen participation during the OER on the BSCF, we performed operando ^{18}O isotope labeling measurements to monitor the changes in oxygen products throughout the OER process via the use of an on-line mass spectrometer (MS).[21] The extent to which lattice

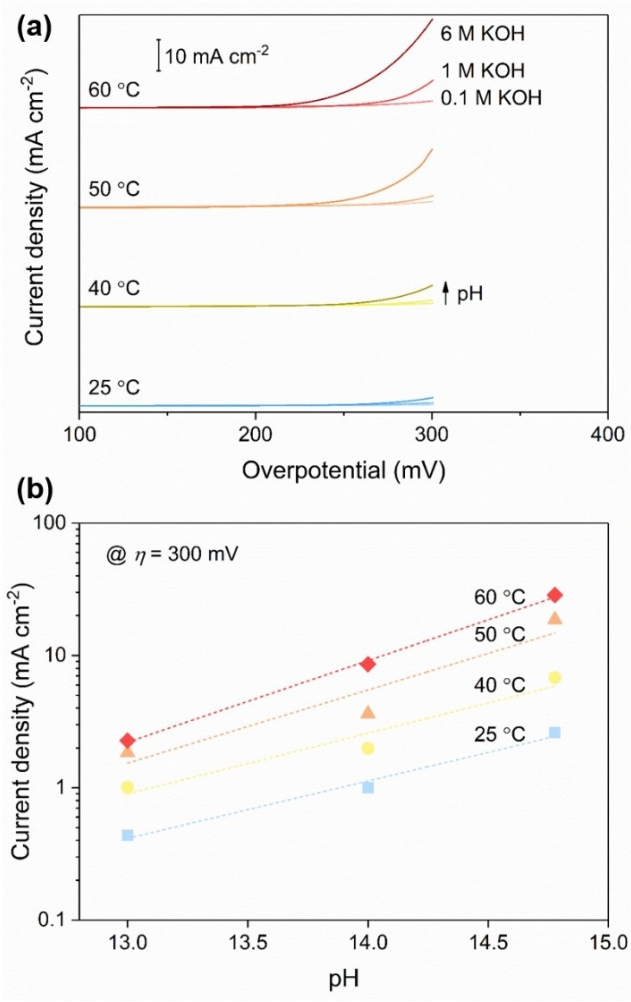

Figure 2. pH dependence under different temperatures. (a) OER kinetic currents under varying pH conditions. (b) Logarithmic representation of OER current density at a 300 mV overpotential in relation to pH.

oxygen participates in the OER can be appraised by comparing the intensity of the MS signal for $m/z = 34$ (corresponding to $^{34}O_2$, i.e., $^{16}O^{18}O$, where ^{18}O originates from a lattice oxygen site that is labeled by the ^{18}O isotope prior to the OER experiment). To account for the natural isotopic abundance of ^{18}O (~0.2%), the background contributions to the $^{34}O_2$ signal were subtracted to reflect the real lattice oxygen participation, as presented in Figure 3 (also see the original data obtained with and without ^{18}O isotope labeling in Figure S4). Significantly, the $^{34}O_2$ signal exhibits a greater intensity at increased temperatures, providing direct evidence to the more favorable LOM pathway on the BSCF under elevated temperatures. Note that the earlier onset (as indicated by the arrows in Figure 3) observed at higher temperatures further indicates the improved OER kinetics with increasing temperature, which agrees well with the results presented in Figure 1.

It was reported that the mobility of oxygen within an oxide catalyst can assume a crucial role in the LOM-catalyzed OER process as it could allow for the ready supply of lattice oxygen to participate in the OER.[19] Using electrochemical methods

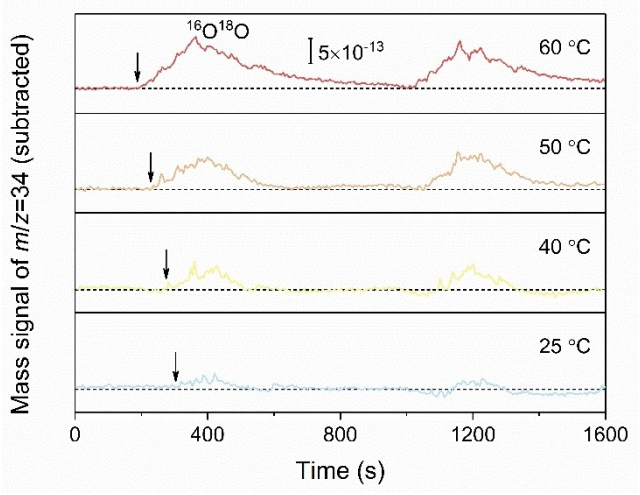

Figure 3. Mass signals of $^{34}O_2$ ($^{16}O^{18}O$) during the OER over ^{18}O-labeled BSCF in Ar-purged 1 M KOH at various temperatures. Background signals from control samples without ^{18}O labeling were subtracted.

established earlier,[22] we tested the oxygen ion diffusion coefficient (D_O) of BSCF at various temperatures as a measure to compare the oxygen mobility. The oxygen intercalation and de-intercalation properties were first assessed by cyclic voltammetry (CV) in an Ar-saturated 1 M KOH. As shown in Figure 4a, redox peaks, indicative of the intercalation and de-intercalation of oxygen ions, can be discerned in the CV curves before the onset of OER currents.[23] Notably, the intensity of such redox peaks became larger at higher temperatures, signifying a greater propensity for oxygen intercalation/de-intercalation.[23a] Chronoamperometry (CA) tests were then conducted to determine the D_O values by employing a previously established bounded three-dimensional diffusion model.[22] It was found that the D_O value exhibited an increase, rising from 1.66×10^{-12} cm^2 s^{-1} at 25 °C to 3.24, 5.32, and 10.00×10^{-12} cm^2 s^{-1} at temperatures of 40, 50, and 60 °C, respectively. Additionally, when plotting the logarithm of oxygen ion diffusion coefficient ($\log D_O$) against the reciprocal temperature (1000/T), an Arrhenius relationship emerged as follows:

$$\log D_O = -2.297 \times 10^3/T - 4.136 \text{ cm}^2 \text{ s}^{-1} \quad (2)$$

From this Arrhenius relationship, an activation energy of 44.0 kJ mol^{-1} could be derived for the diffusion process (Figure 4b). The increased oxygen diffusivity at elevated temperatures is likely beneficial to the LOM process on BSCF.

Combining these results, it is believed that the increased OER activity of BSCF with increasing temperature is primarily a result of the greater extent of lattice oxygen participation, which was facilitated by the enhanced oxygen mobility at elevated temperatures. Note that a more favorable LOM-participated OER pathway also agrees with the reduced Tafel slopes observed earlier at higher temperatures.

The capability to stably sustain the OER is a crucial issue for catalysts to be deployed in practical water electrolysis. We therefore evaluated the electrocatalytic OER stability of BSCF

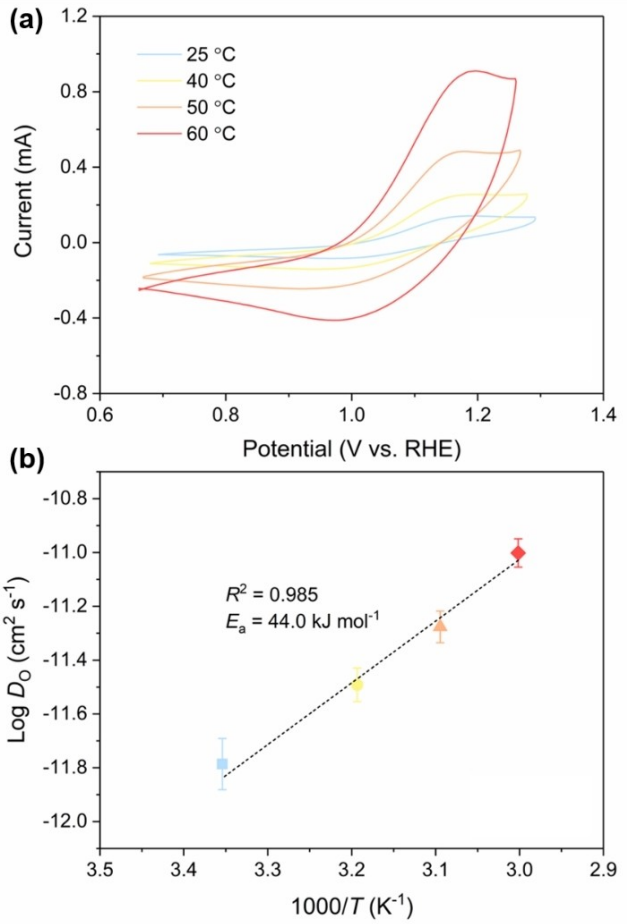

Figure 4. Oxygen ion diffusivity of BSCF measured in Ar-saturated 1 M KOH at elevated temperatures. (a) CV curves of BSCF where redox peaks indicate the electrochemical intercalation and de-intercalation of oxygen ions. (b) Arrhenius relationship of reciprocal temperature versus logarithm of oxygen ion diffusion coefficient. Error bars depict data obtained from a minimum of three replicates.

through continuous CV cycling tests. Figure 5 shows the OER kinetic currents at different CV scans taken for the GCE-supported BSCF catalyst at typical temperature conditions (i.e., near-room temperature of 25 °C and elevated temperature of 60 °C). It was observed that at low temperature, the OER activity initially exhibited an increase with cycling and then approached a steady state (after ~10 scans), followed by some certain decline upon prolonged cycling (30–50 scans). However, when it comes to high-temperature operation, the OER activity only underwent a decrease process, implying the instability of the BSCF catalyst at elevated temperatures. Of note, such a phenomenon was consistently observed across all pH conditions studied here. In addition, for both low- and high-temperature cases, testing under a more strongly alkaline environment (like 1 M and 6 M KOH) tends to cause an activity loss somewhat more severe compared to that under a mildly alkaline condition (e.g., 0.1 M KOH). These observations suggest that BSCF becomes less stable when subjected to near-industrial testing conditions (i.e., high temperatures and high electrolyte concentrations). A similar trending was also found

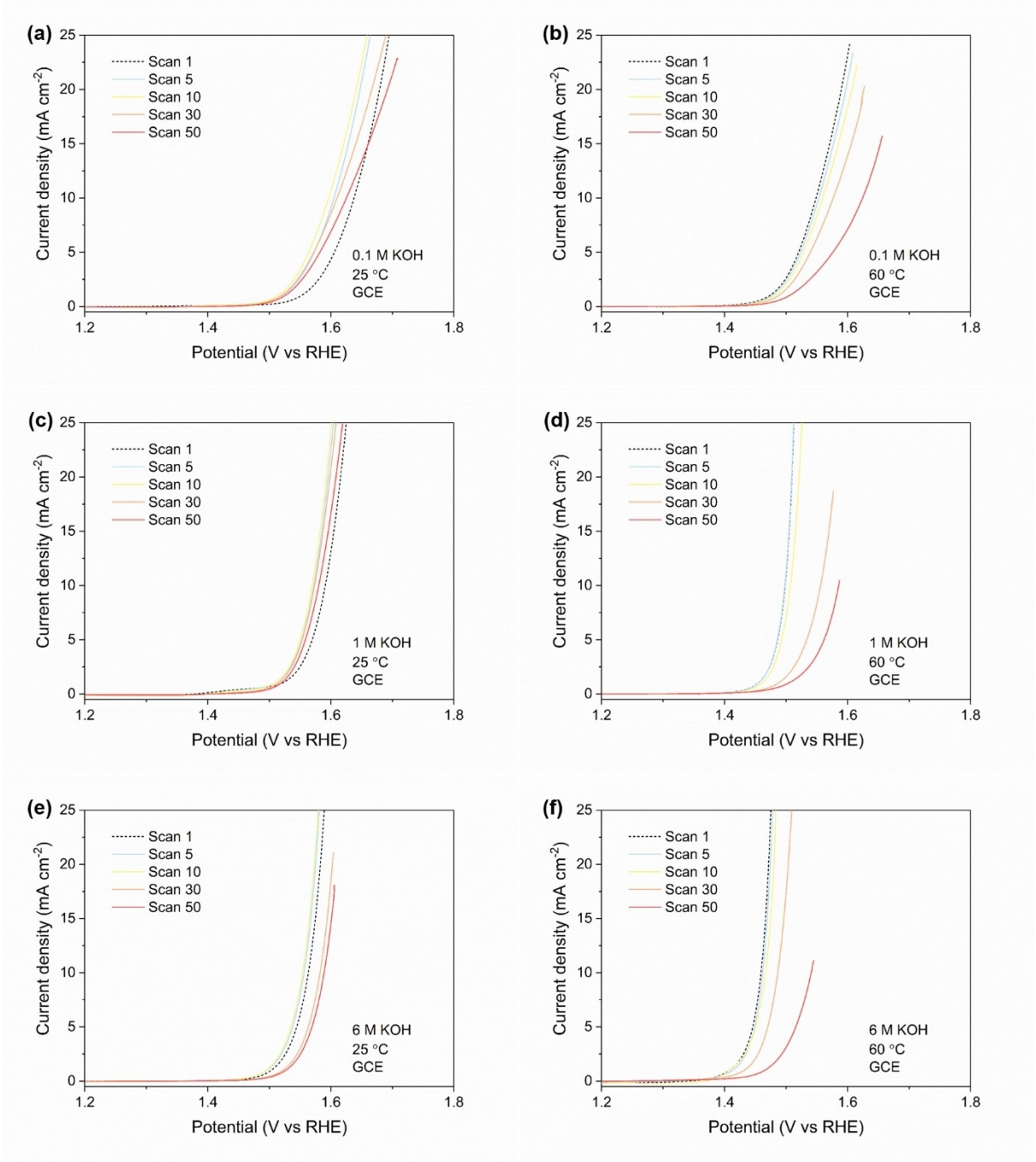

Figure 5. OER kinetic currents at different CV scans taken at 25 and 60 °C. (a–b) In 0.1 M KOH. (c–d) In 1 M KOH. (e–f) In 6 M KOH. Data were collected using BSCF catalyst supported on a GCE substrate.

when BSCF was loaded on a carbon paper substrate to allow for even more extended cycling (up to 100 scans) in 1 M KOH (Figure S5).

Previous studies indicated that upon OER cycling, even under mild conditions (i.e., at room temperature and in a 0.1 M KOH solution), perovskite oxide catalysts utilizing the LOM mechanism would readily undergo surface amorphization along with the leaching of A-site cations (such as Ba^{2+} and Sr^{2+}),[14a,15,19] which could account for the above-mentioned stability trend observed at 25 °C. Here we further show that with increasing temperature, such surface amorphization and cation leaching become more pronounced (which is more so under a greater pH condition), which is responsible for the catalytic instability at a higher temperature of 60 °C. Considering the difficulty in directly quantifying the amount of cations leached during the OER in KOH solutions, which is often associated with the exceedingly low loading of catalyst and hence the extremely low amount of cations that can possibly dissolve, we primarily resorted to analyze the leaching via inductively coupled plasma-optical emission spectrometry (ICP-

OES) using BSCF samples that were intentionally subjected to extended treatments (for 5 h) under different temperature and electrolyte conditions (Table S1). As depicted in Figure 6a, the relative amount of Ba^{2+}/Sr^{2+} leached increased monotonically with increasing temperature for BSCF samples treated in pure water. A same trend was found for samples treated in KOH solutions with increasing pH, and the leaching in 6 M KOH was much more severe compared with that in 0.1 M and 1 M KOH. We further analyzed the leaching via inductively coupled plasma-mass spectrometry (ICP-MS), which offers a lower detection limit than ICP-OES does, on BSCF samples that were subjected to OER cycling at various temperatures (Table S2). Similarly, it was found that the leaching of Ba^{2+}/Sr^{2+} became more pronounced at elevated temperatures. If one considers the leaching (and the accompanying amorphization) to be a result of the reaction between BSCF and water (or KOH solution), the extended treatments mentioned earlier could actually give rise to an enlargement of the BSCF's surface area, similar to what was observed for BSCF samples treated in hydrogen peroxide solutions.[24] Indeed, N_2 sorption measurements revealed an increasing tendency of surface area with increasing temperature and KOH concentration (Figure 6b and Table S3), which further supports the more pronounced cation leaching and surface amorphization.

To more directly observe the surface amorphization, we performed high-resolution transmission electron microscopy (HRTEM) on BSCF samples cycled in different KOH solutions at a high temperature of 60 °C (Figure 7). As a control, the BSCF cycled at a mild pH and temperature condition (0.1 M KOH and 25 °C) was also measured, showing an almost crystalline surface with a limited amount of amorphization, which is consistent with the CV cycling result presented in Figure 5a and the previous report.[14a] After OER cycling at 60 °C, a greater degree of surface amorphization was found in 0.1 M KOH, which became further exacerbated when cycled in 1 M and 6 M KOH. In particular, a surface amorphous layer measuring as large as ~20 nm in thickness was observed for BSCF cycled in 6 M KOH. These observations provide direct evidence of the significantly increased extent of surface amorphization with increasing KOH concentration. It is noted that the occurrence of surface amorphization may have an adverse effect on the oxygen ion diffusion, causing an insufficient supply of lattice oxygen during the LOM-catalyzed OER process and hence the deterioration of the catalytic activity of BSCF, in particular, under harsh conditions such as at a high temperature of 60 °C (and at a high pH).

To summarize, BSCF was found to show significantly improved OER activity when operating at elevated temper-

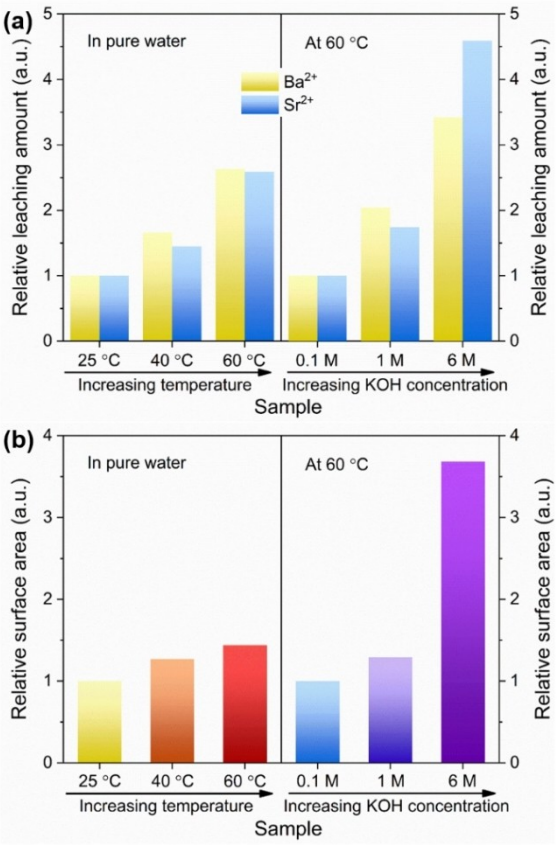

Figure 6. Surface amorphization and cation leaching of BSCF at elevated temperatures. (a) Relative leaching amount of Ba^{2+}/Sr^{2+} and (b) relative surface area for BSCF samples treated in pure water at different temperatures and at 60 °C in different KOH solutions. To aid the comparison, the leaching amount and surface area at high temperatures (40 and 60 °C) and in high-concentration KOH solutions (1 M and 6 M) were reported as relative to those at low temperature (25 °C) and in low-concentration KOH solution (0.1 M), respectively.

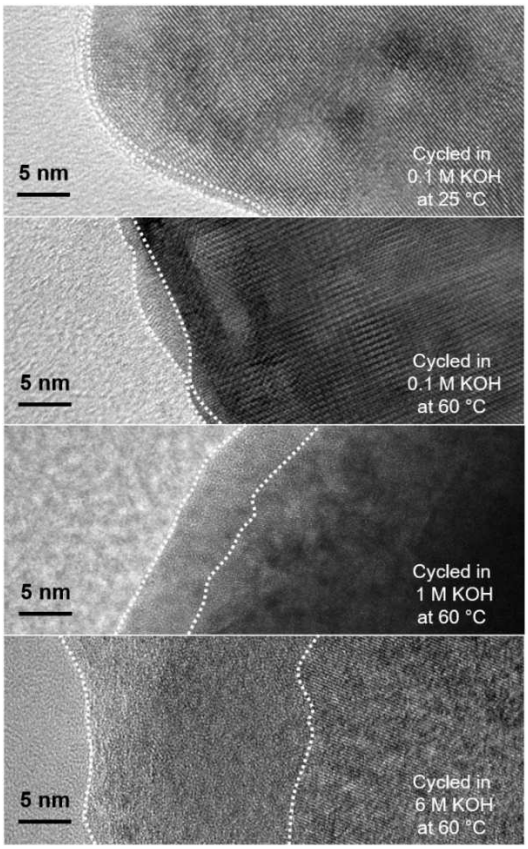

Figure 7. HRTEM images of BSCF samples subjected to OER cycling at 60 °C under various pH conditions, in comparison to that cycled at 25 °C in 0.1 M KOH.

atures due to substantially enhanced lattice oxygen participation, which, however, also led to more pronounced surface amorphization and cation leaching and consequently attenuated OER stability (Figure 8).

Conclusions

In conclusion, this study elucidates for the first time how the well-known BSCF perovskite catalyzes the OER under high-temperature conditions akin to the industrial setting. It was found that BSCF experienced a significant increase of OER activity with increasing temperature, due to the enhanced lattice oxygen participation at elevated temperatures. It was also observed that with increasing temperature, the surface amorphization and cation leaching of BSCF became more severe, causing a considerable activity loss upon extended OER cycling. To mitigate the stability challenge, future research efforts may focus on rationally developing more stable catalyst structure, or on intentionally adding A-site cations in solutions to inhibit dissolution. We expect that our results can provide guidance for research into the fundamental OER catalysis under near-industrial conditions, which can promote the development of real-world electrolyzers such as the AEMWE.

Experimental Section

Catalyst Synthesis and Treatment

BSCF was prepared using a sol–gel technique as described in detail by our group previously.[14c] The precursor obtained from the sol–gel process was subjected to calcination at 1000 °C for a duration of 5 hours to yield the BSCF oxide. To study the leaching of Ba^{2+}/Sr^{2+} cations, the as-prepared BSCF sample was subjected to heat treatment in pure water at temperatures of 25, 40, and 60 °C for 5 h and in KOH solutions with concentrations of 0.1, 1, and 6 M at 60 °C for 5 h. The amount of BSCF was kept the same for each treatment. After treatment, filtration was performed. The filtrate was collected and subsequently analyzed using ICP-OES to quantify the Ba^{2+}/Sr^{2+} concentration, while the dried, treated BSCF powder was subjected to N_2 sorption measurements for analyzing the specific surface area.

Characterizations

Phase structure of BSCF was determined using XRD conducted on a powder diffractometer (D8 Advance, Bruker, Germany) with a Cu Kα radiation source (wavelength: 1.5418 Å). Cation leaching was analyzed by ICP-OES (Optima 7300 DV, PerkinElmer). Specific surface area was calculated from the Brunauer-Emmett-Teller (BET) method using N_2 sorption analysis (TriStar II PLUS, Micromeritics). Surface structure of BSCF was evaluated by HRTEM on a microscope (G2 80–200, FEI Titan) operating at 200 kV.

Electrochemical Measurements

The electrocatalytic OER performance was evaluated in an RDE-based three-electrode setup with most of the parts purchased from Pine Research Instrumentation, Inc. (USA). A Pt wire served as the counter electrode and was positioned within a fritted glass tube to ensure isolation from the electrolyte solution. A mercury oxide (Hg/HgO) was employed as the reference electrode, which was linked to the bulk electrolyte via a salt bridge to prevent any potential adverse effects resulting from the elevated electrolyte temperatures. A catalyst-coated GCE (0.196 cm^2) with a PEEK shroud was used as the working electrode. A water-jacketed electrolytic cell was adopted, whose temperature was controlled by a thermostatic water bath circulator (Temperature Controller, AMETEK Brookfield TC-102) and further confirmed by a thermometer. The BSCF catalyst was loaded onto the GCE (pre-polished to a mirror finish) by casting a 5 μL portion of a well-mixed catalyst ink, which was made by sonicating for 1 h a blend of 10 mg of BSCF, 2 mg of carbon black (Super P®, Alfa Aesar), 900 μL of absolute ethanol, and 100 μL of binder solution (5 wt% Nafion® 117, Sigma-Aldrich), resulting in an estimated BSCF mass loading of approximately 0.25 mg cm^{-2}. Electrolytes of different concentrations (0.1, 1, and 6 M) were prepared by dissolving potassium hydroxide pellets (99.99%, Sigma-Aldrich) in ultrapure water (18.2 MΩ cm).

Ultrapure O_2 (99.999%, Coregas) was purged to achieve O_2 saturation and to ensure the O_2/H_2O equilibrium prior to the experiment at each temperature. Afterwards, the OER activity was recorded on a CHI760E electrochemical workstation (CH Instruments, Inc., USA) by running CV curves at a scan rate of 10 mV s^{-1} with the RDE rotated at 2,400 rpm to avoid any possible accumulation of the evolved O_2 bubbles on the electrode surface. The anodic and cathodic scans were taken average to obtain the OER kinetic currents, which were then normalized by the geometric surface area of the GCE. The potential was compensated for ohmic losses using the electrolyte resistance obtained from electrochemical impedance spectroscopy tested on CHI760E. All reported potentials were converted from the Hg/HgO scale to the reversible hydrogen electrode (RHE) scale by conducting experiments detailed elsewhere.[25] Using a three-electrode setup with Pt foil serving as both the working electrode and counter electrode and Hg/HgO as the reference electrode, CV was carried out at a slow scan rate of 1 mV s^{-1}. The thermodynamic potential (vs Hg/HgO) was determined as the average of the potentials at which the current crossed zero. The overpotential (η) was calculated using the following equation:

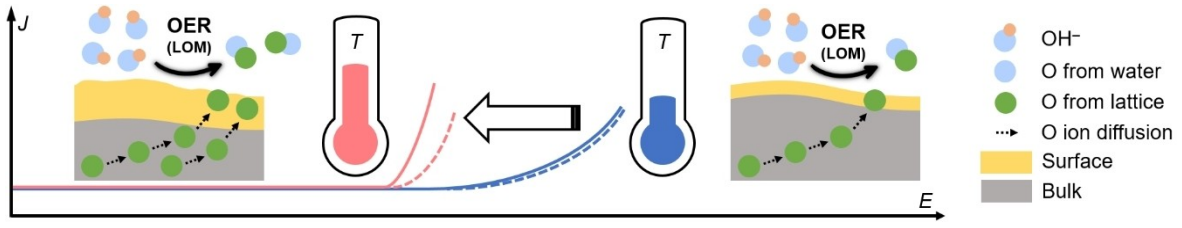

Figure 8. Schematic illustration showing how elevating the operating temperature would lead to increased involvement of lattice oxygen in the OER process on BSCF, which is responsible for the enhanced OER activity as well as the attenuated OER stability. *J*: Current. *E*: Potential. *T*: Temperature. Solid curves represent the initial OER kinetic currents whereas dashed curves represent the kinetic currents after OER cycling.

$$\eta = E - E^0 \quad (3)$$

Here, E is the applied potential and E^0 is the O_2/H_2O equilibrium potential (in V) calculated from the following:[26]

$$E^0 = \left(\frac{-\Delta G^0_{O_2/H_2O}(T)}{2F}\right) \quad (4)$$

where F is the Faraday constant and $\Delta G^0_{O_2/H_2O}(T)$ (in J mol^{-1}) is temperature dependent and can be obtained by the below equation (where T is in Kelvin temperature):

$$\Delta G^0_{O_2/H_2O}(T) = -295600 - 33.5T\ln(T) + 388.4T \quad (5)$$

To assess the leaching of Ba^{2+}/Sr^{2+} cations under electrochemical OER conditions at various temperatures, a carbon paper supported BSCF electrode (with an intentionally higher BSCF mass loading of 10 mg cm^{-2}) was subjected to continuous CV cycling in a 0.1 M KOH solution at 100 mV s^{-1} for 100 scans, after which the electrolyte was settled and taken for ICP-MS analysis (Agilent 7800).

^{18}O Isotope Labeling Experiment

The ^{18}O isotope labeling experiment was conducted using a water-jacketed, gas-tight H-type cell connected with an online MS (ThermoStar, Pfeiffer Vacuum) to analyze the gas signals. The H-type cell was separated by a Nafion-117 membrane (Fuel Cell Store). Ultrapure argon (99.999%, Coregas) was purged into this system serving as a carrier gas. The operating temperature was controlled by the same water bath circulator mentioned earlier. The BSCF sample was first deposited on a carbon paper substrate (oxide mass loading: 1 mg cm^{-2}) and then subjected to a chronopotentiometry test at a constant current density of 10 mA cm^{-2} for 30 min in a 1 M KOH solution containing ^{18}O isotope (prepared using water containing $\geq$98 atom% ^{18}O, Taiyo Nippon Sanso) to incorporate the ^{18}O atoms into the BSCF lattice. CV was then performed at 2 mV s^{-1} in an OER potential range of 0.8 V using the ^{18}O-labeled BSCF catalyst as working electrode in a fresh 1 M KOH electrolyte (prepared with ultrapure water in the absence of ^{18}O). As a control, the same experiment was performed on the BSCF catalyst without ^{18}O isotope labeling, whose background contributions to the $^{34}O_2$ signal due to the natural isotopic abundance of ^{18}O in water (~0.2%) were subtracted to unveil the genuine contributions from the lattice oxygen participation in OER.[18a,21a]

Oxygen Ion Diffusion Coefficient Measurement

The measurement of the oxygen ion diffusion coefficient was conducted using an RDE-based three-electrode setup in an Ar-saturated 1 M KOH electrolyte. A combination of CV and CA techniques was applied. The same glass cell and water bath circulator were utilized to maintain the electrolyte temperature. The same Pt wire counter electrode, Hg/HgO reference electrode, and catalyst-modified GCE working electrode were employed. CV was taken at a scan rate of 10 mV s^{-1} with the GCE held stationary. Subsequently, CA was conducted at potentials 10 mV more anodic than the potential of the oxidation peak (as observed in the CV curve) to ensure diffusion-limited intercalation while the GCE was rotated at 2,400 rpm to eliminate any mass-transfer effects arising from the electrolyte.[23b] The calculation of the oxygen ion diffusion coefficient (D_O) was based on the equation below, utilizing a bounded three-dimensional diffusion model:[22]

$$\lambda = a(D_O t)^{-1/2} \quad (6)$$

Here, λ, a dimensionless shape factor, was assumed to be 2, which is representative of a rounded parallelepiped, an intermediate form between a sphere ($\lambda = 1.77$) and a cube ($\lambda = 2.26$).[19,23a] a, radius of the perovskite particle, was approximated using the relationship $S = 6/(2a\rho)$ based on a simplified spherical geometry approximation, where ρ is the theoretical density and S is the BET surface area of BSCF. $t^{-1/2}$ was determined as the intercept (at $i = 0$) from the linear fit of the i vs. $t^{-1/2}$ plot derived from the CA data.

Acknowledgements

This work was supported by the Australian Research Council Discovery Projects (Grant Nos. ARC DP200103332, ARC DP200103315, and ARC DP230100685), Industrial Transformation Research Hubs (Grant No. ARC IH220100012), and Discovery Early Career Researcher Award (Grant No. ARC DE240101013). F.A. would like to acknowledge the Egyptian Ministry of Higher Education and Scientific Research, Cultural Affairs and Missions Sector, Egypt for a PhD scholarship. Open Access publishing facilitated by Curtin University, as part of the Wiley - Curtin University agreement via the Council of Australian University Librarians.

Conflict of Interests

The authors declare no conflict of interest.

Data Availability Statement

The data that support the findings of this study are available from the corresponding author upon reasonable request.

Keywords: elevated temperature · lattice oxygen participation · oxygen evolution reaction · perovskite · water splitting

[1] A. G. Olabi, M. A. Abdelkareem, *Renewable Sustainable Energy Rev.* **2022**, *158*, 112111.
[2] a) A. Hauch, R. Küngas, P. Blennow, A. B. Hansen, J. B. Hansen, B. V. Mathiesen, M. B. Mogensen, *Science* **2020**, *370*, eaba6118; b) Z. Yan, J. L. Hitt, J. A. Turner, T. E. Mallouk, *Proc. Natl. Acad. Sci. USA* **2020**, *117*, 12558–12563; c) D. Sun, X. Xu, Y. Qin, S. P. Jiang, Z. Shao, *ChemSusChem* **2020**, *13*, 39–58; d) H. Xu, Y. Ma, J. Chen, W.-X. Zhang, J. Yang, *Chem. Soc. Rev.* **2022**, *51*, 2710–2758; e) H. Xie, Z. Zhao, T. Liu, Y. Wu, C. Lan, W. Jiang, L. Zhu, Y. Wang, D. Yang, Z. Shao, *Nature* **2022**, *612*, 673–678.
[3] a) X. Xu, Z. Shao, S. P. Jiang, *Energy Technol.* **2022**, *10*, 2200573; b) W. Li, H. Tian, L. Ma, Y. Wang, X. Liu, X. Gao, *Mater Adv* **2022**, *3*, 5598–5644; c) D. Guan, B. Wang, J. Zhang, R. Shi, K. Jiao, L. Li, Y. Wang, B. Xie, Q. Zhang, J. Yu, Y. Zhu, Z. Shao, M. Ni, *Energy Environ. Sci.* **2023**, *16*, 4926–4943; d) M. R. Domalanta, J. N. Bamba, D. D. Matienzo, J. A. del Rosario-Paraggua, J. Ocon, *ChemSusChem* **2023**, *16*, e202300310; e) F. A. Ghafar, D. Etherton, S. Liu, C. E. Buckley, N. J. English, D. S. Silvester, M. V. Sofianos, *J. Electrochem. Soc.* **2022** *169*, 096507.
[4] M. David, C. Ocampo-Martínez, R. Sánchez-Peña, *J. Energy Storage* **2019**, *23*, 392–403.
[5] T. Wang, X. Cao, L. Jiao, *Carb. Neutrality* **2022**, *1*, 21.

[6] S. A. Lee, J. Kim, K. C. Kwon, S. H. Park, H. W. Jang, *Carbon Neutralization* **2022**, *1*, 26–48.
[7] N. Du, C. Roy, R. Peach, M. Turnbull, S. Thiele, C. Bock, *Chem. Rev.* **2022**, *122*, 11830–11895.
[8] a) F. Abdelghafar, X. Xu, S. P. Jiang, Z. Shao, *Mater. Rep. Energy* **2022**, *2*, 100144; b) R. R. Raja Sulaiman, W. Y. Wong, K. S. Loh, *Int. J. Energy Res.* **2022**, *46*, 2241–2276.
[9] H. Sun, X. Xu, Y. Song, W. Zhou, Z. Shao, *Adv. Funct. Mater.* **2021**, *31*, 2009779.
[10] a) J. Hwang, R. R. Rao, L. Giordano, Y. Katayama, Y. Yu, Y. Shao-Horn, *Science* **2017**, *358*, 751–756; b) X. Xu, W. Wang, W. Zhou, Z. Shao, *Small Methods* **2018**, *2*, 1800071.
[11] J. Suntivich, K. J. May, H. A. Gasteiger, J. B. Goodenough, Y. Shao-Horn, *Science* **2011**, *334*, 1383–1385.
[12] X. Xu, C. Su, Z. Shao, *Energy Fuels* **2021**, *35*, 13585–13609.
[13] a) H. Sun, X. Xu, H. Kim, W. Jung, W. Zhou, Z. Shao, *Energy Environ. Mater.* **2023**, *6*, e12441; b) J. Tang, X. Xu, T. Tang, Y. Zhong, Z. Shao, *Small Methods* **2022**, *6*, 2201099; c) B. Deng, G. Yu, W. Zhao, Y. Long, C. Yang, P. Du, X. He, Z. Zhang, K. Huang, X. Li, H. Wu, *Energy Environ. Sci.* **2023**, *16*, 5210.
[14] a) K. J. May, C. E. Carlton, K. A. Stoerzinger, M. Risch, J. Suntivich, Y.-L. Lee, A. Grimaud, Y. Shao-Horn, *J. Phys. Chem. Lett.* **2012**, *3*, 3264–3270; b) J.-I. Jung, H. Y. Jeong, M. G. Kim, G. Nam, J. Park, J. Cho, *Adv. Mater.* **2015**, *27*, 266–271; c) X. Xu, Y. Pan, W. Zhou, Y. Chen, Z. Zhang, Z. Shao, *Electrochim. Acta* **2016**, *219*, 553–559; d) G. Chen, W. Zhou, D. Guan, J. Sunarso, Y. Zhu, X. Hu, W. Zhang, Z. Shao, *Sci. Adv.* **2017**, *3*, e1603206; e) B.-J. Kim, E. Fabbri, D. F. Abbott, X. Cheng, A. H. Clark, M. Nachtegaal, M. Borlaf, I. E. Castelli, T. Graule, T. J. Schmidt, *J. Am. Chem. Soc.* **2019**, *141*, 5231–5240; f) T.-H. Shen, L. Spillane, J. Vavra, T. H. M. Pham, J. Peng, Y. Shao-Horn, V. Tileli, *J. Am. Chem. Soc.* **2020**, *142*, 15876–15883; g) B.-J. Kim, E. Fabbri, M. Borlaf, D. F. Abbott, I. E. Castelli, M. Nachtegaal, T. Graule, T. J. Schmidt, *Mater Adv* **2021**, *2*, 345–355.
[15] E. Fabbri, M. Nachtegaal, T. Binninger, X. Cheng, B.-J. Kim, J. Durst, F. Bozza, T. Graule, R. Schäublin, L. Wiles, M. Pertoso, N. Danilovic, K. E. Ayers, T. J. Schmidt, *Nat. Mater.* **2017**, *16*, 925–931.
[16] B. Zhang, Q. Daniel, M. Cheng, L. Fan, L. Sun, *Faraday Discuss.* **2017**, *198*, 169–179.
[17] a) Y. Sun, L. Yuan, Z. Liu, Q. Wang, K. Huang, S. Feng, *Mater. Chem. Front.* **2019**, *3*, 1779–1785; b) E. Nurlaela, T. Shinagawa, M. Qureshi, D. S. Dhawale, K. Takanabe, *ACS Catal.* **2016**, *6*, 1713–1722.
[18] a) A. Grimaud, O. Diaz-Morales, B. Han, W. T. Hong, Y.-L. Lee, L. Giordano, K. A. Stoerzinger, M. T. M. Koper, Y. Shao-Horn, *Nat. Chem.* **2017**, *9*, 457–465; b) L. Giordano, B. Han, M. Risch, W. T. Hong, R. R. Rao, K. A. Stoerzinger, Y. Shao-Horn, *Catal. Today* **2016**, *262*, 2–10.
[19] Y. Pan, X. Xu, Y. Zhong, L. Ge, Y. Chen, J. M. Veder, D. Guan, R. O'Hayre, M. Li, G. Wang, H. Wang, W. Zhou, Z. Shao, *Nat. Commun.* **2020**, *11*, 2002.
[20] a) X. Xu, Y. Pan, Y. Zhong, C. Shi, D. Guan, L. Ge, Z. Hu, Y.-Y. Chin, H.-J. Lin, C.-T. Chen, H. Wang, S. P. Jiang, Z. Shao, *Adv. Sci.* **2022**, *9*, 2200530; b) C. Yang, C. Laberty-Robert, D. Batuk, G. Cibin, A. V. Chadwick, V. Pimenta, W. Yin, L. Zhang, J.-M. Tarascon, A. Grimaud, *J. Phys. Chem. Lett.* **2017**, *8*, 3466–3472; c) X. Xu, Y. Pan, L. Ge, Y. Chen, X. Mao, D. Guan, M. Li, Y. Zhong, Z. Hu, V. K. Peterson, M. Saunders, C. T. Chen, H. Zhang, R. Ran, A. Du, H. Wang, S. P. Jiang, W. Zhou, Z. Shao, *Small* **2021**, *17*, e2101573; d) H. Zhang, Y. Gao, H. Xu, D. Guan, Z. Hu, C. Jing, Y. Sha, Y. Gu, Y.-C. Huang, Y.-C. Chang, C.-W. Pao, X. Xu, J.-F. Lee, Y.-Y. Chin, H.-J. Lin, C.-T. Chen, Y. Chen, Y. Guo, M. Ni, W. Zhou, Z. Shao, *Adv. Funct. Mater.* **2022**, *32*, 2207618.
[21] a) D. Guan, H. Xu, Q. Zhang, Y.-C. Huang, C. Shi, Y.-C. Chang, X. Xu, J. Tang, Y. Gu, C.-W. Pao, S.-C. Haw, J.-M. Chen, Z. Hu, M. Ni, Z. Shao, *Adv. Mater.* **2023**, *35*, 2305074; b) H. Zhang, D. Guan, Z. Hu, Y.-C. Huang, X. Wu, J. Dai, C.-L. Dong, X. Xu, H.-J. Lin, C.-T. Chen, W. Zhou, Z. Shao, *Appl. Catal. B* **2021**, *297*, 120484.
[22] a) F. R. Van Buren, G. H. J. Broers, A. J. Bouman, C. Boesveld, *J. Electroanal. Chem. Interfacial Electrochem.* **1978**, *87*, 389–394; b) F. R. Van Buren, G. H. J. Broers, A. J. Bouman, C. Boesveld, *J. Electroanal. Chem. Interfacial Electrochem.* **1978**, *88*, 353–361.
[23] a) J. T. Mefford, X. Rong, A. M. Abakumov, W. G. Hardin, S. Dai, A. M. Kolpak, K. P. Johnston, K. J. Stevenson, *Nat. Commun.* **2016**, *7*, 11053; b) R. P. Forslund, W. G. Hardin, X. Rong, A. M. Abakumov, D. Filimonov, C. T. Alexander, J. T. Mefford, H. Iyer, A. M. Kolpak, K. P. Johnston, K. J. Stevenson, *Nat. Commun.* **2018**, *9*, 3150.
[24] C. Su, X. Xu, Y. Chen, Y. Liu, M. O. Tadé, Z. Shao, *J. Power Sources* **2015**, *274*, 1024–1033.
[25] X. Xu, Y. Chen, W. Zhou, Z. Zhu, C. Su, M. Liu, Z. Shao, *Adv. Mater.* **2016**, *28*, 6442–6448.
[26] U. A. Paulus, T. J. Schmidt, H. A. Gasteiger, R. J. Behm, *J. Electroanal. Chem.* **2001**, *495*, 134–145.

Manuscript received: October 21, 2023
Revised manuscript received: March 10, 2024
Accepted manuscript online: March 12, 2024
Version of record online: April 6, 2024